Stabilization of an ambient-pressure collapsed tetragonal phase in $CaFe_2As_2$ and tuning of the orthorhombic-antiferromagnetic transition temperature by over 70 K via control of nanoscale precipitates

S. Ran,[1] S. L. Bud'ko,[1] D. K. Pratt,[1] A. Kreyssig,[1] M. G. Kim,[1] M. J. Kramer,[2] D. H. Ryan,[3] W. N. Rowan-Weetaluktuk,[3] Y. Furukawa,[1] B. Roy,[1] A. I. Goldman,[1] and P. C. Canfield[1]

[1]*Ames Laboratory, U.S. DOE and Department of Physics and Astronomy, Iowa State University, Ames, Iowa 50011, USA*

[2]*Ames Laboratory, U.S. DOE and Department of Materials Science and Engineering, Iowa State University, Ames, Iowa 50011, USA*

[3]*Centre for the Physics of Materials and Physics Department, McGill University, Montreal, Quebec, H3A 2T8 Canada*

(Received 23 January 2011; revised manuscript received 22 February 2011; published 19 April 2011)

We have found a remarkably large response of the transition temperature of $CaFe_2As_2$ single crystals grown from excess FeAs to annealing and quenching temperature. Whereas crystals that are annealed at 400°C exhibit a first-order phase transition from a high-temperature tetragonal to a low-temperature orthorhombic and antiferromagnetic state near 170 K, crystals that have been quenched from 960°C exhibit a transition from a high-temperature tetragonal phase to a low-temperature, nonmagnetic, collapsed tetragonal phase below 100 K. By use of temperature-dependent electrical resistivity, magnetic susceptibility, x-ray diffraction, Mössbauer spectroscopy, and nuclear magnetic resonance measurements we have been able to demonstrate that the transition temperature can be reduced in a monotonic fashion by varying the annealing or quenching temperature from 400° to 850°C with the low-temperature state remaining antiferromagnetic for transition temperatures larger than 100 K and becoming collapsed tetragonal, nonmagnetic for transition temperatures below 90 K. This suppression of the orthorhombic-antiferromagnetic phase transition and its ultimate replacement with the collapsed tetragonal, nonmagnetic phase is similar to what has been observed for $CaFe_2As_2$ under hydrostatic pressure. Transmission electron microscopy studies indicate that there is a temperature-dependent width of formation of $CaFe_2As_2$ with a decreasing amount of excess Fe and As being soluble in the single crystal at lower annealing temperatures. For samples quenched from 960°C there is a fine (of order 10 nm) semiuniform distribution of precipitate that can be associated with an average strain field, whereas for samples annealed at 400°C the excess Fe and As form mesoscopic grains that induce little strain throughout the $CaFe_2As_2$ lattice.

DOI: 10.1103/PhysRevB.83.144517 PACS number(s): 74.70.Xa, 61.50.Ks, 64.75.Nx, 75.30.−m

I. INTRODUCTION

$CaFe_2As_2$ manifests an extreme example of the coupled magnetic-structural phase transition that epitomizes the physics of the undoped parents of the FeAs-based superconductors.[1,2] The strongly first-order transition at ambient pressure from a high-temperature, tetragonal, paramagnetic phase to a low-temperature, orthorhombic, antiferromagnetic phase takes place near 170 K in single crystals grown from Sn flux and manifests a hysterisis of several degrees as seen in thermodynamic, transport, and microscopic measurements.[1–5]

$CaFe_2As_2$ is also the most pressure sensitive of the AFe_2As_2 and 1111 compounds with its structural-magnetic phase transition being initially suppressed by over 100 K per GPa.[2,6–10] As pressure increases, a nonmagnetic, collapsed tetragonal phase that is stabilized by ∼0.3 GPa intersects and terminates the lower-pressure orthorhombic-antiferromagnetic phase line near 100 K and 0.4 GPa and rises to 300 K by ∼1.5 GPa.[6–8] In addition to this extreme pressure sensitivity, $CaFe_2As_2$ is also very sensitive to nonhydrostaticity.[2,7–12] If the pressure medium solidifies before the structural phase transitions, then the anisotropic changes in the unit cell lead to nonhydrostatic (by definition) stress, which in turn leads to dramatically broadened transitions and a structurally mixed phase sample in the 0.4-GPa pressure region. This mixed phase includes a small amount of strain-stabilized, high-temperature tetragonal phase which superconducts at low temperatures.[2,6–10,12,13] The use of helium as a pressure medium allows for a minimization of these nonhydrostatic effects and has allowed for the determination of the T-P phase diagram.[2,7–9]

Sn-grown single crystals of $CaFe_2As_2$ are highly deformable and join the RSb_2 and RBi_2 compounds[14,15] as rare examples of malleable intermetallic compounds. Single-crystal plates can be bent and, to some extent, even rolled by simply grasping with tweezers and applying minor torques across the sample length by pressing one end of the crystal downward on the surface of the laboratory bench or microscope stage. This malleability can lead to extreme broadening of features in ground samples, as were seen in early attempts at powder x-ray diffraction.[1]

$CaFe_2As_2$ samples were initially grown from Sn and characterized in single-crystal form.[1,5] Sn-grown crystals are well-formed, faceted plates that generally have planar dimensions of several millimeters and thicknesses between 0.1 and 0.5 mm.[1,2] For measurements that require larger sample volumes pseudopolycrystalline[7] or oriented single crystalline assemblies (see Figure 1 in Ref. 16) can be used. Larger single crystals of $CaFe_2As_2$ have been grown from ternary melts rich in FeAs.[8] In order for these larger crystals to manifest a structural-magnetic phase transition similar to that seen in the smaller Sn-grown crystal, they were annealed at 500°C for 24 h (a temperature similar to the decanting temperature of the Sn-grown samples). Without this annealing, the larger, FeAs-grown samples had dramatically suppressed transition temperatures.

Given recent observations of small shifts in the structural and magnetic transition temperatures of $BaFe_2As_2$ samples and of the superconducting transition in doped $BaFe_2As_2$, as well as of sharpenings of their signatures in thermodynamic and transport data,[17,18] we undertook a systematic study of the effects of postgrowth thermal treatment of FeAs-grown single crystals of $CaFe_2As_2$. We have discovered that, once again, $CaFe_2As_2$ is the extreme case in the AFe_2As_2 series, manifesting a surprisingly large suppression of the structural-magnetic transition temperature in as-grown samples (nearly 50%) that, even more remarkably, can be systematically changed from ∼170 K to below 100 K, with the lowest transition temperature samples having a transition into the nonmagnetic, collapsed tetragonal state but at ambient pressure.

In order to characterize and understand the effects of temperature treatment, as well as the nature of the low-temperature state, we have performed a wide variety of thermodynamic, transport, microscopic, and spectroscopic measurements. Temperature-dependent electrical resistivity and magnetic susceptibility measurements were used to determine a transition temperature-annealing temperature (T^*-T_a) phase diagram as well as to identify similarities between the collapsed tetragonal phase and the low-temperature state of FeAs-grown $CaFe_2As_2$ crystals quenched from temperatures between 850° and 960°C. For annealing temperatures $T_a \gtrsim$ 400° C the T^*-T_a phase diagram is found to be remarkably similar to the T^*-pressure (P) phase diagram, bringing up the question of what the relationship between T_a and P could be. Temperature-dependent single-crystal x-ray diffraction measurements were then employed to unambiguously show that the crystallographic phase transition in as grown samples quenched from 960°C is one to a collapsed tetragonal state that is in qualitative as well as quantitative agreement with what is found for Sn-grown samples under applied pressures of ∼0.4 GPa. Temperature-dependent Mössbauer spectroscopy measurements showed that the low-temperature magnetic state of annealed FeAs-grown $CaFe_2As_2$ single crystals remains antiferromagnetic until the transition temperature is suppressed to below 100 K when the low-temperature ground state becomes nonmagnetic, a result confirmed by nuclear magnetic resonance (NMR) measurements. Finally, transmission electron microscopy (TEM) measurements revealed that there is a small, temperature-dependent width of formation for $CaFe_2As_2$, allowing for a solid solubility of excess Fe and As in the single crystals that decreases with temperature. As the quenching temperature is reduced from 960°C to 400°C the initially fine precipitate coarsens, decreasing the degree of strain detected in the sample.

II. EXPERIMENTAL METHODS

Single crystals of $CaFe_2As_2$ were grown from excess FeAs by rapidly cooling a melt of $CaFe_4As_4$ from 1180° to 1020°C over 3 h, slowly cooling from 1020° to 960°C over 35 h, and then decanting off the excess liquid, essentially quenching the samples from 960°C to room temperature. Details of the growth technique can be found in Refs. 19 and 20. These samples will be referred to as "as grown samples." Postgrowth, thermal treatments of samples involve the following variables: annealing temperature, annealing time, and annealing environment. Annealing environment refers to either (i) annealing a whole, unopened, decanted growth ampoule or (ii) annealing individual crystals that have been picked from a growth and resealed in evacuated silica tubes. For studies of the effects of annealing temperature, we seal several crystals into an evacuated silica tube and anneal for 24 h in a furnace stabilized at the specified temperature. The sample is placed into the hot furnace and, after annealing, it is quenched to room temperature. Longer time anneals (7 days) were used to prepare whole, unopened batches of samples. In order to study the effects of annealing on FeAs-grown samples with transition temperatures (and features) like the Sn-grown crystals, samples that had been annealed for a week at 400°C were subsequently sealed into an evacuated silica tube and annealed for 24 h in a furnace stabilized at the specified temperature. Although a detailed study of the annealing time dependence of sample changes will need to be done in the future, we found that, for example, at 450°C a 1-h anneal is not enough to effect complete change, but anneals longer than 4 h do not lead to any further significant changes in sample behavior; at 800°C annealing appears to be completed in under 0.5 h.

Temperature-dependent magnetization measurements were made in a Quantum Design (QD) Magnetic Property Measurement System unit. Temperature-dependent electrical resistivity was measured in a four-probe configuration, with Pt wires attached to the samples by Du Pont 4929N Ag paint (cured at room temperature), in a QD Physical Property Measurement System unit. Although normalized resistivity values are plotted, the resistivity values of samples did not vary outside the uncertainty associated with a combination of geometric error (associated with measuring dimensions of the sample) and difficulties associated with sample exfoliation. The average room-temperature resistivity of as-grown 700°C annealed and 400°C annealed samples was 3.75±0.75 mΩ cm (a 20% variation).

In order to identify the nature of the structural transition in the as-grown $CaFe_2As_2$ crystal (quenched from 960°C) and to determine the temperature dependence of the lattice parameters, high-energy x-ray diffraction measurements (E = 99.62 keV) using an area detector were performed on the 6-ID-D station in the Midwest Universities Collaborative Access Team Sector at the Advanced Photon Source. At this high energy, x rays probe the bulk of a crystal rather than just the near-surface region and, by rocking the crystal about both the horizontal and vertical axes perpendicular to the incident x-ray beam, an extended range of a chosen reciprocal plane can be recorded.[21] For the measurements, the horizontal angle, μ, was scanned over a range of ±3.6° for each value of the vertical angle, η, between ±3.6° with a step size of 0.4°. The two-dimensional scattering patterns were measured by a MAR345 image plate positioned 1503 mm behind the sample. The crystal was mounted on the cold finger of a closed-cycle refrigerator surrounded by a beryllium heat shield and vacuum containment. Additionally, the crystal was mounted such that there was access to ($hk0$), ($h0l$), and (hhl) reciprocal lattice planes. The (008) and (220) peaks were fit for lattice parameter determination and, for these measurements, the total exposure time for each frame was 383 s.

The Mössbauer absorbers were prepared by attaching several single-crystal plates to a 12-mm-diameter disk of 100-μm-thick Kapton foil using GE-7031 varnish. The spaces between the crystals were filled with a radio-opaque paint prepared by mixing 1-5 μm tungsten powder (obtained from Alpha-Aesar) with diluted GE-7031 varnish. The absence of gaps in the completed mosaic was confirmed first visually and then by looking for transmission of the 6.4-keV Fe-K_α x ray from the ^{57}Co Mössbauer source. In the configuration used, the crystalline c axis was parallel to the Mössbauer γ beam.

The Mössbauer spectra were collected on a conventional spectrometer using a 50-mCi ^{57}Co/Rh source mounted on an electromechanical drive operated in constant acceleration mode. The spectrometer was calibrated against α-Fe metal at room temperature. Temperatures down to 5 K were obtained using a vibration-isolated closed-cycle refrigerator with the sample in a partial pressure of helium to ensure thermal uniformity. Spectra were fitted using a conventional, nonlinear, least-squares minimization routine to a sum of equal-width Lorentzian lines. The line positions for the magnetic sextets observed in the ordered state were calculated assuming first-order perturbation in order to combine the effects of the magnetic hyperfine field and the electric-field gradient. As the samples were oriented mosaics rather than powders, the line intensities were constrained to be in the ratio 3:R:1:1:R:3 (following the conventional practice of labeling the lines from negative to positive velocity)[22] with the intensities of the two $\Delta m_I = 0$ lines being variable (R) to allow for the expected magnetic texture. $R = 0$ would correspond to the moments being parallel to the Mössbauer γ beam, whereas $R = 4$ indicates that the moments are perpendicular to the beam.

Nuclear magnetic resonance (NMR) measurements were carried out on ^{75}As ($I = 3/2$; $\gamma/2\pi = 7.2919$ MHz/T) by using a homemade phase-coherent spin-echo pulse spectrometer to investigate the magnetic and electronic properties of differently treated $CaFe_2As_2$ crystals from a microscopic point of view.^{75}As-NMR spectra at a resonance frequency of 51 MHz were obtained by sweeping the magnetic field.

TEM samples were prepared by mechanically polishing the single crystal to $\sim$10 μm thick along the c axis and then ion milling to perforation using 3 keV $\sim 18^\circ$ incident angle and following up with 30 min at 500 eV at 10° to remove milling damage. All milling was performed using a liquid N_2 cooled stage (sample $T \sim 120$ K). Samples were analyzed using a Philips CM30 TEM operated at 300 keV. Energy-dispersive spectroscopy (EDS) and selective area diffraction patterns (SADP) were also performed on the samples in the TEM.

III. DATA PRESENTATION

Figure 1 presents the resistivity and magnetic susceptibility for $CaFe_2As_2$ single crystals grown from Sn and for $CaFe_2As_2$ single crystals grown from excess FeAs. Two data sets are shown for FeAs-grown crystals: one data set shows measurements on an as -grown crystal that was decanted at, and quenched from, 960°C; the other data set shows measurements on a sample from a batch that was subsequently annealed at 400°C for a week. The Sn-grown single crystal and the

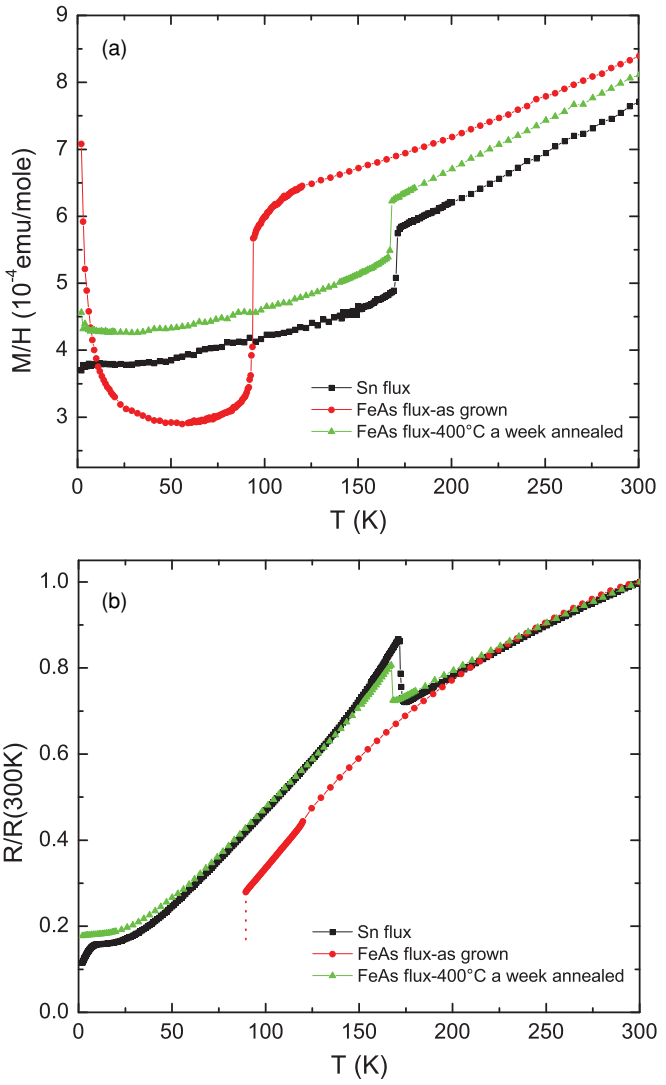

FIG. 1. (Color online) Temperature-dependent (a) magnetic susceptibility and (b) normalized electrical resistivity of $CaFe_2As_2$ for three differently prepared single crystals: (squares) Sn grown, (circles) as grown (quenched from 960°C) from FeAs, and (triangles) FeAs grown, annealed for 1 week at 400°C. Note: when the as-grown sample from FeAs melt was cooled below the transition temperature near 90 K it shattered, making further lower-temperature resistivity measurements impossible.

FeAs-grown sample that has been annealed at 400°C are quite similar, both manifesting similar, modest increases in resistivity and decreases in susceptibility associated with the phase transition near 170 K.[1,2] On the other hand, the FeAs sample that was quenched from 960°C shows a significantly larger, very sharp drop in magnetization occurring well below 100 K. The electrical resistivity also drops discontinuously at this temperature, associated with the sample suddenly undergoing a violent structural phase transition that often (usually) leads to shattering along the length and width of the bar, as well as loss of contacts.

In addition to the quantitative differences shown in Fig. 1, there is a qualitative difference between the as-grown, $CaFe_2As_2$ single crystals from FeAs solution and the single crystals grown from Sn. Whereas the Sn-grown single crystals

are malleable and can easily be bent and deformed, the crystals quenched from a 960°C FeAs solution are brittle and tend to shatter if bending is attempted. The FeAs-grown crystals that have been annealed at 400°C, however, recover some of the malleability of the Sn-grown ones and can deform a little without shattering.

Given the dramatic difference in transition temperature, as well as the different signatures of the transition in resistivity and magnetization, several questions arise. Among them we consider: (i) what is the nature of the phase transition in the as grown sample and (ii) can the transition in annealed samples be varied from near 170 K to below 100 K in a systematic manner? We will address the latter question first and return to the former after the creation of a T^*-T_a phase diagram.

In order to assess the extent to which the 170 K phase transition that occurs in Sn-grown, as well as annealed FeAs-grown, samples of $CaFe_2As_2$ can be systematically shifted down to below 100 K we measured the temperature-dependent susceptibility and resistivity of as grown samples that were annealed for 24 h at temperatures ranging from 250° to 850°C. Figure 2 presents magnetic susceptibility and resistivity data for representative annealing temperatures. The decrease in susceptibility (or increase in resistivity) can be shifted down in temperature by choosing an appropriate annealing temperature between 400° and 800°C. For annealing between these temperatures, the transitions, particularly as seen in the resistivity data, remain quite sharp and shift in a systematic manner. Whereas the size of the jump in the magnetization remains fairly constant in the samples annealed in this temperature region, there is a monotonic increase in the magnitude of the increase in the resistivity (see Fig. 7 below).

Such a clear temperature dependence of the effects of annealing, over such a wide temperature range, begs the question of what the annealing time dependence of these effects is. In other cases of clear annealing effects, both time and temperature cuts through phase space are needed to establish unambiguous annealing protocols.[23] In Fig. 3 we show the evolution of the magnetic susceptibility for different annealing times. At 450°C, 0.5 h is an insufficient amount of time to cause any significant change; 1.0 h leads to split, broadened features with drops in susceptibility below both 170 and 100 K; 3.0 h leads to a single, sharp feature near 170 K, comparable to what is seen for 24-h anneals. This progression shows that for 450°C, 24 h is longer than the salient time scale for annealing. As would be expected, for higher temperatures the salient time scale is even shorter. In Fig. 3(b) samples from a batch that had been annealed for a week at 500°C, with a transition temperature above 150 K, were annealed at 800°C for representative times. As can be seen, even a 0.5-h anneal causes the sample to behave in a manner similar to the as grown (quenched from 960°C) samples.

Figure 2 also demonstrates that 24-h anneals at temperatures of 300°C or lower do not change the temperature dependence of the as-grown samples. The data from the sample annealed at 350°C for 24 h shows somewhat broadened drops in susceptibility near both 170 and 100 K, similar to what was seen for a 1.0-h anneal at 450°C [Fig. 3(a)], indicating that at 350°C 24 h is comparable to, but less than, the salient time scale. Although longer annealing times for $T \lesssim 350$°C may lead to a sharp, single transition near 170 K (as is seen for the 400° and 500°C 24-h anneals), the time needed to achieve this state is anticipated to become exponentially long. The one other data point we can add to this is the fact that 20°C (room temperature) anneals approaching 10^4 h have not led to significant changes in behavior of as-grown samples.

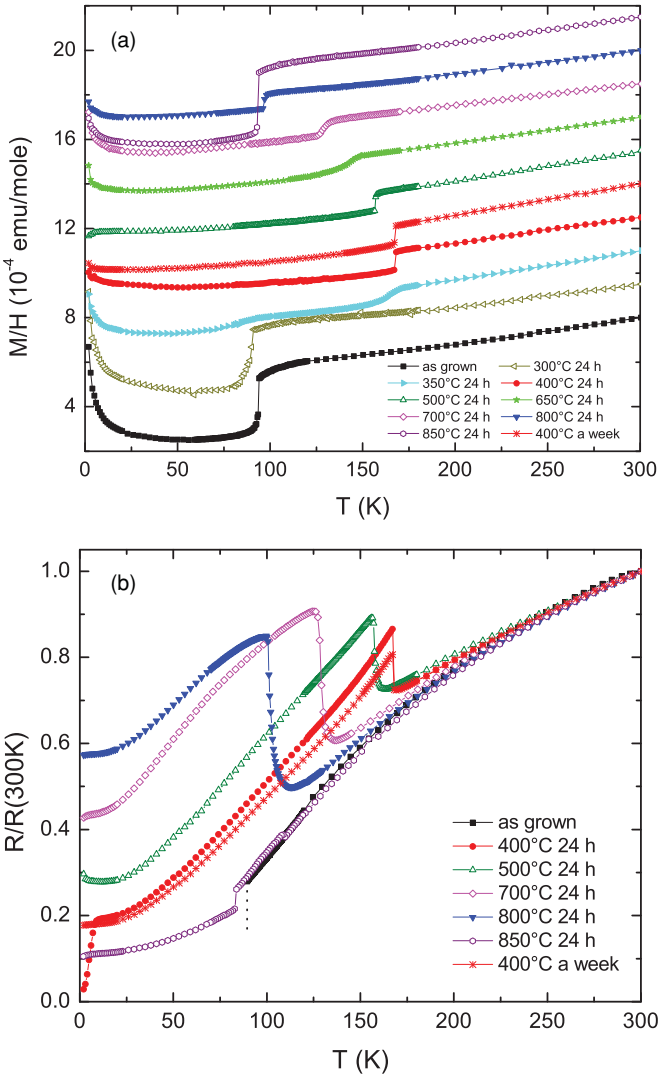

FIG. 2. (Color online) Temperature-dependent magnetic susceptibility and normalized electrical resistivity of as-grown $CaFe_2As_2$ single crystals annealed for 24 h at temperature, T_a. Susceptibility data in (a) have been offset from each other by an integer multiple of 1.5×10^{-4} emu/mole for clarity. Data for a 1-week anneal of a whole batch at 400°C is shown for comparison. The resistivity data (b) for the as-grown sample could not be measured below the transition temperature due to sample breakage, but for the sample annealed at 850°C resistivity could be measured through the transition.

A 24-h anneal at 850°C does not significantly change the transition temperature from that measured for the as-grown samples quenched from 960°C (perhaps not too surprisingly since 850°C is approaching the 960°C quench temperature); the resistivity data for this sample, though, can be collected below the transition temperature, showing that the low-temperature state has a lower resistivity, leading to a downward jump in resistivity when cooling through the transition temperature.

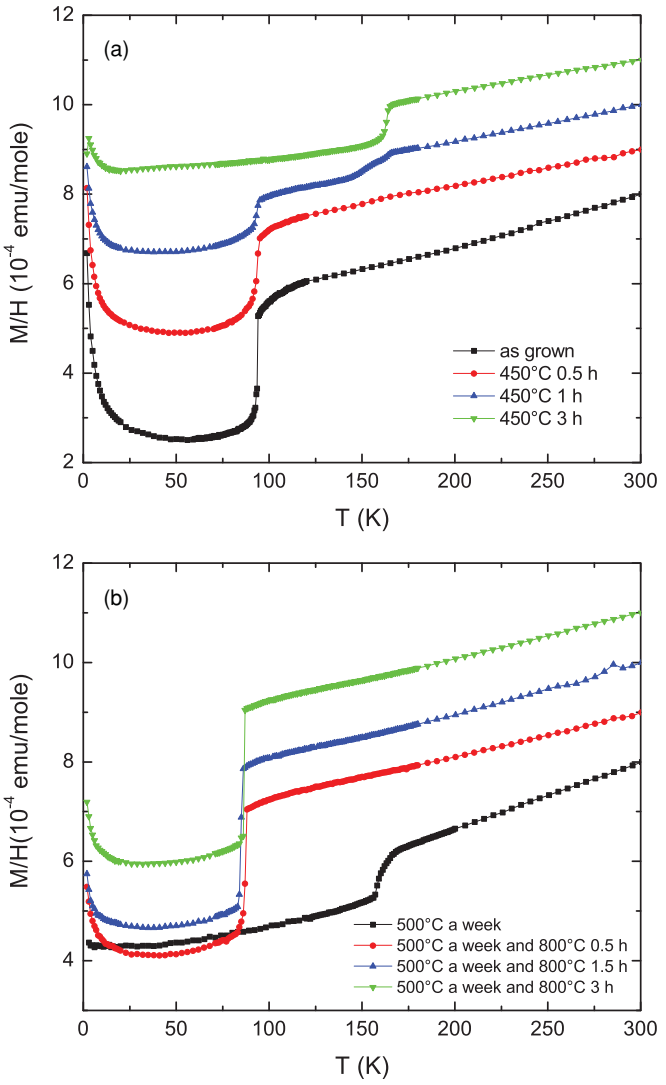

FIG. 3. (Color online) Temperature-dependent magnetic susceptibility of (a) as-grown $CaFe_2As_2$ single crystals annealed at 450°C for representative times and (b) as-grown $CaAs_2Fe_2$ single crystals that have been annealed for a week at 500°C and then annealed at 800°C for representative times. Data in both panels have been offset from each other by an integer multiple of 1×10^{-4} emu/mole for clarity.

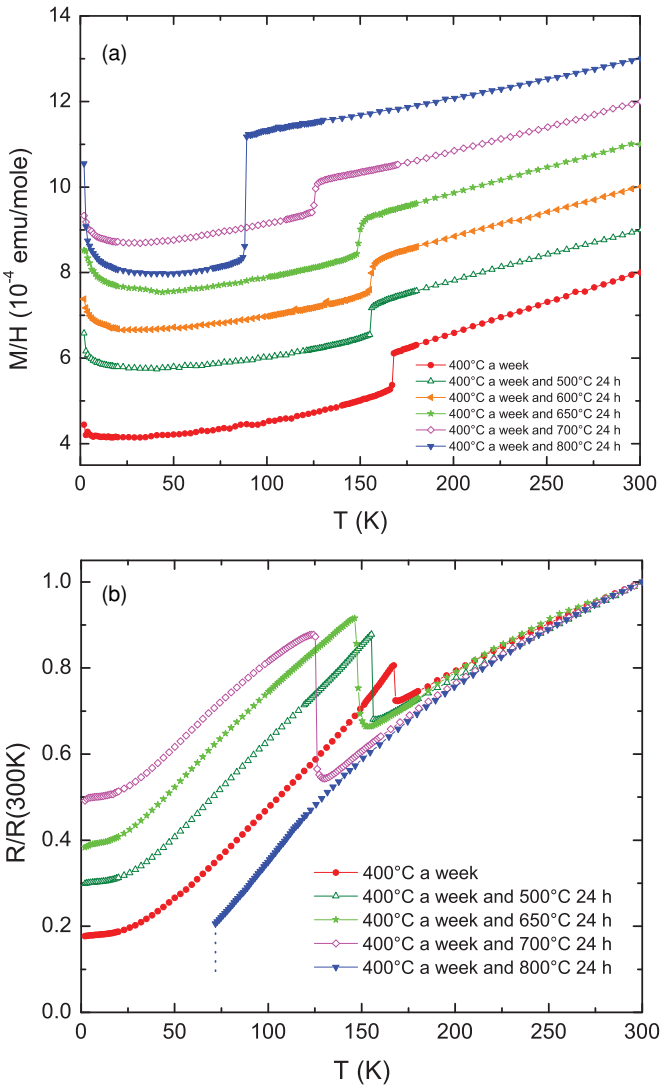

FIG. 4. (Color online) Temperature-dependent (a) magnetic susceptibility and (b) normalized electrical resistivity of as-grown $CaFe_2As_2$ single crystals that were first annealed for a week at 400°C and then annealed for 24 h at temperature, T_a. Susceptibility data in (a) have been offset by an integer multiple of 1×10^{-4} emu/mole from each other for clarity.

In order to see if similar changes in transition temperature could be induced by annealing samples that started with transitions near 170 K (i.e., started with transitions similar to those found in Sn-grown $CaFe_2As_2$), we annealed an entire batch of crystals at 400°C for a week. The resistivity and susceptibility data for these samples are also shown in Fig. 2 and are essentially the same as those found for the 24-h anneal of individual crystals. Single crystals from this "400°C anneal for one week" batch were then separately sealed in silica ampoules and annealed for 24 h at temperature ranging from 500° to 800°C. The temperature-dependent resistivity and susceptibility for these samples are shown in Fig. 4. As was the case for the as grown samples, sharp features in both resistivity and susceptibility systematically shift to lower temperature when the sample is annealed at higher temperature. The sample annealed at 800°C shows the larger drop in susceptibility and broke on cooling through its transition, making it appear to be similar to the as grown, quenched from 960°C, samples.

Figure 5 presents the transition temperature-annealing temperature, T^*-T_a, plot. Figure 6 illustrates how values for T^*, as well as the error bars, were inferred from the resistivity and susceptibility data. As can be seen in Figs. 2 and 4, for $T_a > 400$°C, there is a systematic progression of fairly sharp transitions downward for increasing T_a. Figure 5 illustrates that (i) there is some scatter in T^* for a given T_a, but (ii) that there is also a fairly well-defined suppression of T^* with increasing T_a, e.g., a 400°C anneal gives a very different transition temperature from a 700°C anneal, which itself differs from a 850°C anneal or the as-grown sample. In addition, annealing at a given T_a leads to a T^* value, regardless of whether the sample starts from a 170 K or ~90 K transition state, i.e., this final anneal determines T^* regardless of sample history.

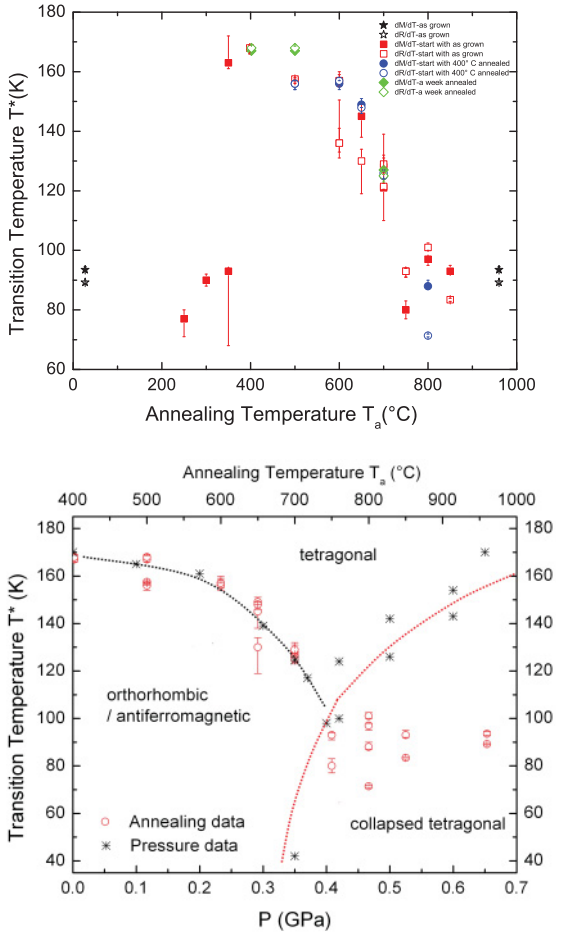

FIG. 5. (Color online) (a) Transition temperature-annealing temperature (T^*-T_a) phase diagram. Open symbols are inferred from resistivity data and filled symbols are inferred from susceptibility data. (Star) The as-grown samples (quenched from 960°C data and are also shown as 20°C anneals); (squares) as-grown samples that have been annealed for 24 h at T_a and quenched to room temperature; (circles) as-grown samples that were first annealed for a week at 400°C and then annealed for 24 h at T_a and quenched to room temperature; and (diamonds) as-grown samples that have been annealed for a week as whole, unopened batches at T_a. (b) T^* as a function of pressure from Ref. [9] and T^* as a function of T_a for 400°C $\leqslant T_a \leqslant$ 960°C.

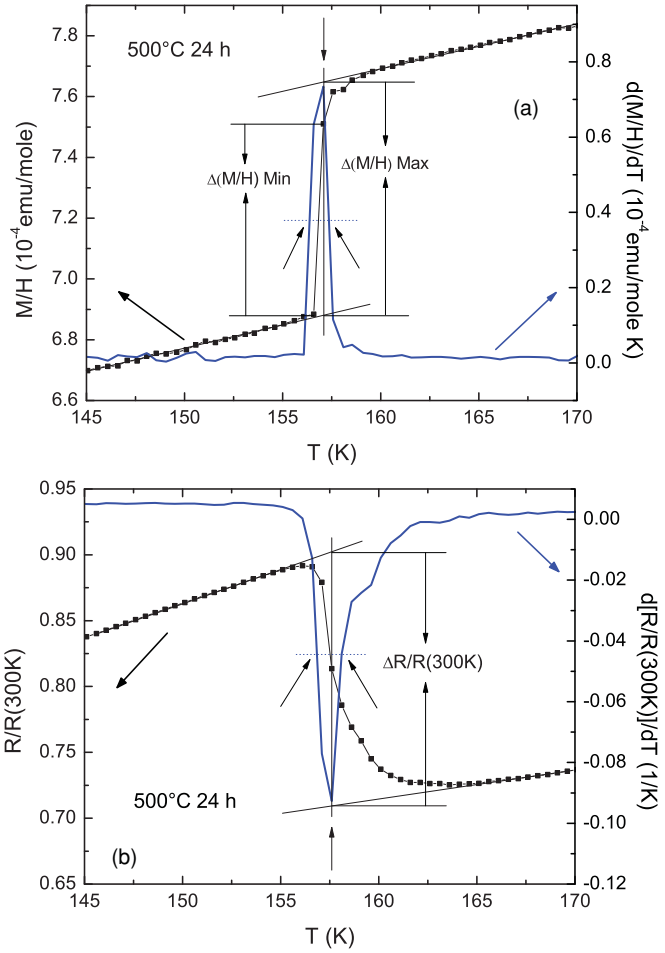

FIG. 6. (Color online) Temperature-dependent (a) magnetic susceptibility and (b) normalized electrical resistivity and their respective temperature derivatives for an as grown crystal annealed at 500°C for 24 h. T^* is inferred from the temperature of the extremum in the derivative. Full width at half maximum of derivative is used to define error bars shown in Fig. 5. Values of the jump in magnetic susceptibility (maximum and minimum values) and resistivity are inferred as shown.

The T^*-T_a phase diagram presented in Fig. 5 shows that $CaFe_2As_2$ grown from FeAs can have the temperature of its phase transition modified in an essentially continuous manner from near 170 K to below 100 K. For transitions with T^* between 170 K and 100 K the magnetic signature of the transition is essentially unchanged and the resistive signature evolves gradually with the jump in resistivity, $\Delta\rho$, becoming larger as T^* decreases. For the lowest T^* values, below 100 K, there is a significantly larger drop in susceptibility and, when it can be measured, the jump in resistivity is downward on cooling rather than upward. These observations are quantified in Fig. 7. As discussed in the previous section, the room-temperature resistivity of as-grown samples as well as those annealed at 400° and 700°C for a week all have room-temperature resistivity values of 3.75 ±0.75 mΩ cm. This invariance, within experimental resolution, allows for conversion of these jumps to absolute resistivity as needed.

The evolution of the transition temperature (Fig. 5) as well as the evolution of the resistive and magnetic signature of the phase transition (Figs. 1– 4) make it plausible that for 170 K > $T^* \gtrsim$ 100 K the transition is similar to that seen in Sn-grown $CaFe_2As_2$: a transition from a high-temperature, tetragonal, paramagnetic state to a lower-temperature, orthorhombic, antiferromagnetic state. On the other hand, dramatic changes in the resistive and magnetic signature associated with the as grown sample as well as samples annealed near 850°C are consistent with our current understanding of the collapsed tetragonal phase, a phase that up until this time was associated with $CaFe_2As_2$ under pressures of 0.35 GPa or higher. The change in the resistive signature of the transition from a sharp increase to a sharp decrease, as well as the sudden increase in the size of the drop in susceptibility upon cooling are very similar to the changes seen in Ref. 9 under hydrostatic pressure applied with helium. For that matter, the basic phase

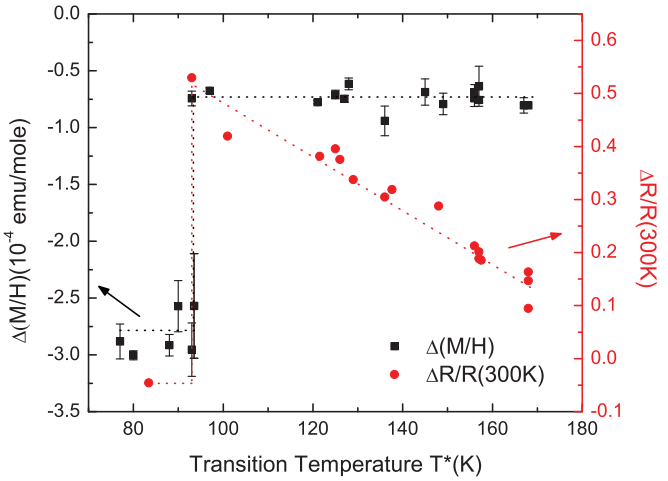

FIG. 7. (Color online) Size of jump in susceptibility and normalized resistivity as a function of transition temperature for FeAs-grown $CaFe_2As_2$ crystals annealed at temperatures shown in Figures 1– 4. Room-temperature resistivity of samples with T^* values of ∼ 90, 130, and 170 K all fall within the 3.75±0.75 mΩ cm range.

diagram proposed in Refs. 8 and 9 is remarkably similar to the $T_a > 400^\circ$C part of the T^*-T_a phase diagram presented in Fig. 5, with T_a playing the role of pressure or, more precisely stated, somehow parameterizing the amount of stress in the sample. This similarity can be seen in Fig. 5(b), which directly plots T^* as a function of P and T_a. For annealing temperatures that allow for the achievement of equilibrium by 24 h (i.e., 400°C or greater) there is a remarkable agreement between the effects of T_a and P on T^*, at least as long as the transition is from high-temperature tetragonal to low-temperature orthorhombic, antiferromagnetic. Once the low-temperature state is the nonmagnetic, collapsed tetragonal phase the annealing temperature does not seem to affect T^* in the same manner as P.

Before progressing too much further, though, we need to examine (and, as will be shown, verify) several of the hypotheses outlined above. First, we should parametrize and understand the nature of the low-temperature ground state in the as-grown FeAs crystals. Once that is done we can return to the question of what may be causing the systematic changes we see in the T^*-T_a phase diagram.

The collapsed tetragonal, CT, phase was identified[7,8] in $CaFe_2As_2$ by scattering measurements made on samples under hydrostatic pressure using He as a pressure medium as part of a comprehensive effort to better understand the details of the $CaFe_2As_2$ T-P phase diagram.[6–9,11] As $CaFe_2As_2$ transforms from the high-temperature tetragonal phase into the low-temperature, collapsed tetragonal phase the c-lattice parameter changes from ∼11.6 Å to ∼10.6 Å, a remarkably large (∼10%) decrease while the a-lattice parameter increases by ∼2%, leading to an ∼4% decrease in the unit cell volume.[7] In order to see if the as-grown sample manifests such a striking change in lattice parameters, high-energy single-crystal x-ray diffraction data were collected as a function of temperature. Figure 8 displays the results of fits to these data to extract the lattice parameters [Figs. 8(a) and 8(b)] as well as the unit cell volume [Fig. 8(c)]. The data from the original Sn-flux-grown

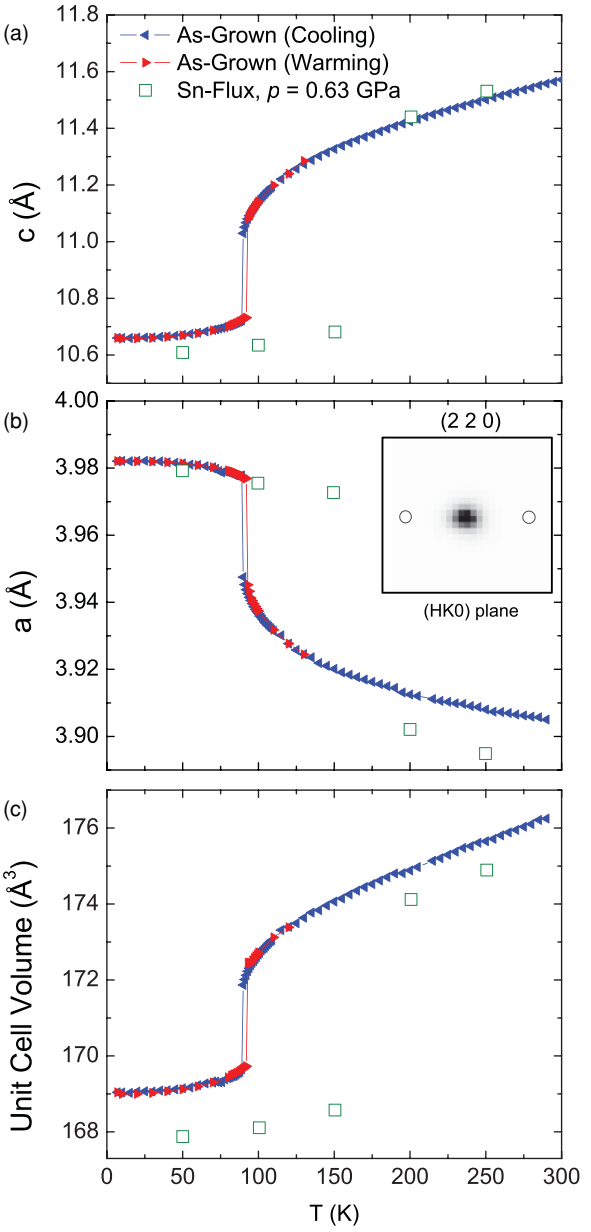

FIG. 8. (Color online) Values for (a) the c-lattice paramter, (b) a-lattice parameter, and (c) unit cell volume as a function of temperature for an unannealed FeAs flux-grown $CaFe_2As_2$ sample determined from high-energy x-ray diffraction measurements. The open squares denote the results of measurements performed on a polycrystalline sample under applied hydrostatic pressure of 0.63 GPa from Ref. 7. The inset to the middle panel is the image of the (220) diffraction peak taken from the two-dimensional x-ray detector as described in the text. Note the absence of any splitting that would signal a transition to an orthorhombic phase [the two open circles illustrate the expected distance between split Bragg peaks due to the "usual" orthorhombic distortion].

samples, at an applied pressure of 0.63 GPa,[7] are also included in Fig. 8 for direct comparison. These data clearly indicate that, structurally, the as-grown crystals of $CaFe_2As_2$ transform into a collapsed tetragonal phase below 100 K at ambient pressure. In particular, the inset to Fig. 8(b) shows the diffraction image of the (220) Bragg reflection at 6 K, the base temperature of

our measurement. Within our resolution, no splitting of the peak is evident as would be expected for an orthorhombic unit cell. Furthermore, we find that the temperature dependence of the lattice parameters and unit cell volume are consistent with what was observed for the pressure-induced, collapsed tetragonal phase for $P = 0.63$ GPa where the tetragonal-to-CT phase transition has moved above 150 K.

Although the sharp drop in susceptibility certainly suggests that the nonmagnetic phase is associated with the collapsed tetragonal state, it is prudent to examine the magnetic properties of this state more closely with microscopic measurement techniques. Mössbauer spectroscopy measurements were carried out on three FeAs-grown samples at selected temperatures. Composite samples, with aligned c axes, were made from single crystals from whole batches treated in the following manner: as grown (quenched from 960°C), annealed for a week at 500°C, and annealed for a week at 700°C. As shown in Fig. 5, these three annealing temperatures produce samples representative of the whole range of behavior observed. Whereas similar sample masses were used for the two extreme samples, a smaller sample mass was used for the sample annealed at 700°C, leading to slightly poorer signal and statistics.

The spectra of the three samples taken at 295 K (Fig. 9) are essentially indistinguishable, showing a barely resolved quadrupole split doublet with the high velocity line slightly more than twice the intensity of the lower velocity line in each case. The location of the Fe atoms in the $ThCr_2Si_2$-type structure requires that the principal axis of the local electric field gradient tensor lies along the c axis, so our oriented mosaic should yield an intensity ratio of 3:1,[22] rather than the 2.3(3):1, 2.0(2):1, and 2.4(2):1 observed here for the 500°C annealed, 700°C annealed, and as-grown samples, respectively. It is unlikely that the reduced ratio is due to misalignment of the crystal plates as the intensities in the magnetic patterns are consistent with almost-perfect alignment. It is possible

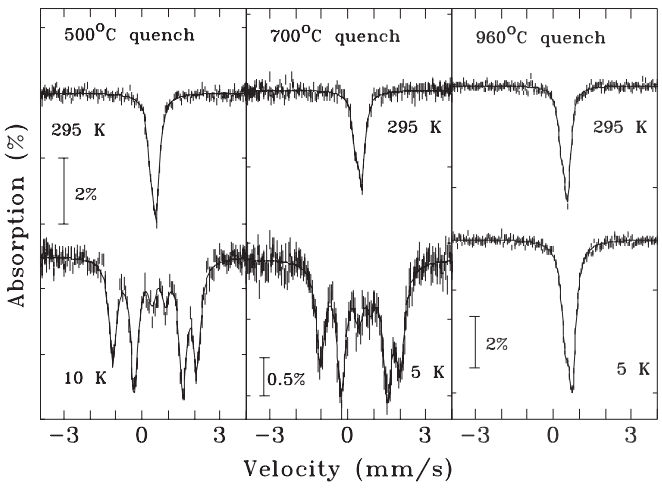

FIG. 9. ^{57}Fe Mössbauer spectra of an *ab*-plane single-crystal mosaic of samples (from left) annealed at 500°C, annealed at 700°C, and as-grown (quenched from 960°C). In each case the upper spectrum was taken at 295 K, whereas the lower spectrum was taken at 10 K or 5 K. Only the as-grown sample shows no magnetic ordering at base temperature. The solid lines are fits as described in the text.

that a minor impurity is the source of the reduced ratio; however, no identifiable impurity contribution was found in the residual patterns of the fitted spectra, except in the case of the 700°C annealed sample, where about 4% of the total iron was found to be associated with a nonmagnetic phase at 5 K. The quadrupole splittings for the as-grown and 700°C annealed samples were slightly higher [+0.236(5) mm/s] than that in the 500°C annealed sample [+0.202(12) mm/s] probably reflecting more distorted local Fe environments. The sign of the electric field gradient cannot normally be determined from a ^{57}Fe Mössbauer spectrum of a powder sample but the combination of oriented $ThCr_2Si_2$-type single-crystal samples with the observed intensity ratio makes the sign determination unambiguous.

Cooling to low temperatures makes the differences between the three samples strikingly obvious. The two annealed samples undergo sudden transitions near 170 K (annealed at 500°C) and 130 K (annealed at 700°C) and by 10 K the sample annealed at 500°C has developed a clear magnetic splitting of 10.03(3) T, whereas the sample annealed at 700°C exhibits a slightly smaller hyperfine field of 9.51(3) T. Fitting the intensities of the two $\Delta m_I = 0$ lines (lines 2 and 5) in both magnetic patterns yields $R = 3.8(1)$, implying an almost-perfect (better than 10°) alignment of the crystal c axis with the γ beam,[22] as expected from the construction of the sample and confirming that the ordering direction of the iron moments in both ordered samples lies in the ab plane. By contrast, the spectrum of the as-grown sample is almost unchanged. The quadrupole splitting increases slightly, to 0.272(4) mm/s, and there is also a small increase in linewidth [from 0.143(4) mm/s to 0.170(3) mm/s], possibly reflecting some increased disorder or strain. The largest change appears in the line intensity ratio, which drops to 1.70(7):1 on cooling to 5 K, suggesting either a reduction in quality of the c-axis alignment or a tilting of the principal axis of the local electric field gradient away from the c axis. Remarkably, the original intensity ratio is recovered on warming back to 295 K, so the change is fully reversible. Visual inspection of the three mosaics following several thermal cycles between room temperature and the base temperature of the cryostat did not reveal any apparent damage.

The temperature dependence of the hyperfine field for the two annealed samples, shown in Fig. 10, reveals that not only is the iron moment probably slightly smaller in the sample annealed at 700°C but also the temperature dependence of the hyperfine field (B_{hf}) is visibly stronger, consistent with a lower ordering temperature. Although it is not possible to determine the ordering temperature of the hypothetical, second-order phase transition of an antiferromagnetically ordered, orthorhombic phase transforming into a paramagnetic, orthorhombic phase directly, since in reality the sample undergoes a strong first-order transition to the tetragonal phase on warming, we can make an estimate by fitting the observed temperature dependence of B_{hf} to a Brillouin function as is shown in Fig. 10. This procedure yields estimated ordering temperatures of 300(10) K for the sample annealed at 500°C, and 230(10) K for the sample annealed at 700°C, with the errors dominated by an uncertainty in the effective total angular-momentum quantum number, J, used in the fits. We note that, whereas the absolute values of the Néel temperatures

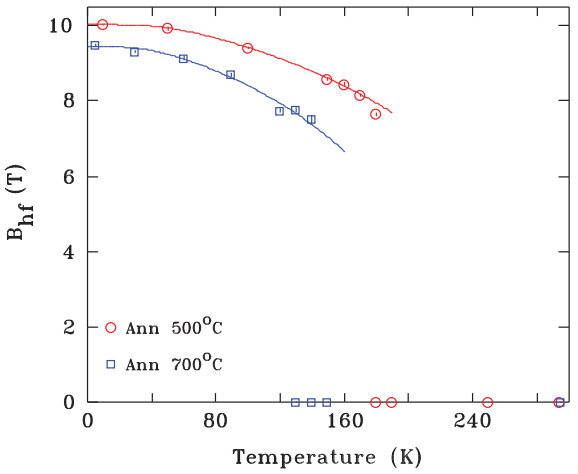

FIG. 10. (Color online) Temperature dependence of the magnetic hyperfine fields (B_{hf}) for the two annealed samples shown in Fig. 9. The solid lines are fits to Brillouin functions (as described in the text) used to estimate the Néel temperatures of the low-temperature, antiferromagnetic, orthorhombic form of each sample. In both cases the samples undergo a first-order structural transition on warming effectively truncating the $B_{hf}(T)$ data.

did depend somewhat on J, the difference between the values of T_N for the two samples did not and was consistently 70(3) K. The magnetic ordering in the sample with the lower structural transition temperature is definitely weaker, involving slightly smaller iron moments.

NMR measurements were also carried out on the as-grown and 400°C annealed samples. Figure 11(a) shows ^{75}As NMR spectra at $T = 200$ K for two magnetic field directions of $H \| c$ axis and $H \| ab$ plane for the 400°C annealed crystal. The observed quadrupole-split NMR spectra are well reproduced by a simple nuclear spin Hamiltonian[24] $H = \gamma\hbar \vec{I} \cdot \vec{H}_{\rm eff} + \frac{h\nu_Q}{6}[3I_Z^2 - I(I+1)]$, where $H_{\rm eff}$ is the effective field at the As site (summation of external field H and the hyperfine field

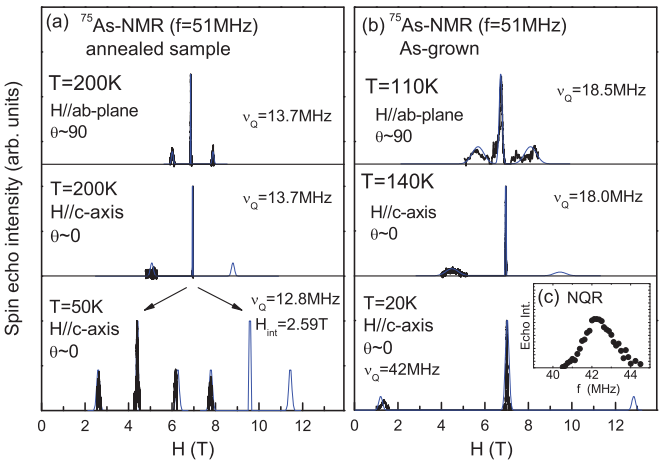

FIG. 11. (Color online) ^{75}As NMR spectra measured at $f = 51$ MHz for (a) 400°C annealed $CaFe_2As_2$ crystal and (b) for the as-grown $CaFe_2As_2$ crystal. Black and blue lines are observed and simulated spectra, respectively. Expected lines above 9 T are not measured due to the limited maximum magnetic field for our SC magnet. (c) ^{75}As NQR spectrum at $T = 4.2$ K and $H = 0$ T.

$H_{\rm int}$), h is Planck's constant, and ν_Q is nuclear quadrupole frequency which is proportional to the electric field gradient (EFG) at the As site (an asymmetric parameter of EFG is assumed to be zero for simplicity). The blue lines in the figure show simulated spectra calculated from the simple Hamiltonian. Below 160 K, each NMR line for $H \| c$ axis splits into two lines due to internal field $H_{\rm int}$ (parallel or antiparallel to H) which is produced by the Fe spin-ordered moment. A typical example of the split NMR lines for $H \| c$ axis is shown at the bottom of Fig. 11(a). The spectrum is reproduced well by $H_{\rm int} = 2.59$ T and $\nu_Q = 12.7$ MHz at $T = 50$ K. These values are in good agreement with previously reported values for ^{75}As NMR of single crystals ($T_N = 167$ K) grown from Sn flux,[25] once again indicating that the sample annealed at 400°C is essentially the same as previously reported ones grown from Sn. The temperature dependence of the ^{75}As spin lattice relaxation rates ($1/T_1$) measured at center line for $H \| c$ axis is also in good agreement with previous work.[25]

Similar quadrupole-split NMR spectra are observed in the as-grown $CaFe_2As_2$ sample as shown in Fig. 11(b), but the observed $\nu_Q \sim 18$–18.5 MHz at $T = 140$–110 K is larger than that in the annealed crystal. The ^{75}As NMR satellite linewidth, which reflects the distribution of EFG, is significantly larger than in the annealed sample, indicative of higher degree of inhomogeneity of the local As environment due to strains, defects, or lattice distortion in the as-grown sample. Below the transition temperature, $T \sim 96$ K, no splitting of the NMR lines is observed (indicating that there is no antiferromagnetic order) but ν_Q is found to change dramatically: from ~18 to ~42 MHz, as is shown at the bottom in Fig. 11(b). Such a drastic change of ν_Q (more than 230%) cannot be explained by thermal expansion of lattice (at most few percentage points) but is attributed to a structural phase transition. The value $\nu_Q \sim 42$ MHz is also confirmed by the observation of nuclear quadrupole resonance (NQR) spectrum at zero magnetic field at $T = 4.2$ K [Fig. 11(c)]. The peak position in the NQR spectrum for the as-grown sample is higher than the 25 and 30.4 MHz for the tetragonal and collapsed tetragonal phases respectively in $CaFe_2As_2$ under high pressure.[26] The combination of no splitting of the NMR lines with the large shift in ν_Q are further confirmation that, for the as-grown sample, there is only a structural phase transition without any magnetic phase transition.

The combination of x-ray diffraction, Mössbauer, and NMR data unambiguously identify the low-temperature state of the as-grown (quenched from 960°C) sample as being nonmagnetic and also having a collapsed tetragonal unit cell that is remarkably similar to what has been found for Sn-grown $CaFe_2As_2$ under hydrostatic pressure. For that matter, the evolution of the temperature-dependent resistivity as well as magnetic susceptibility are both qualitatively similar to the evolutions found when pressure is applied as hydrostatically as possible, i.e., with He as a pressure medium.[9] At this point, not only having created a T^*-T_a phase diagram that looks a lot like the T-P phase diagram (for $T_a > 400$°C) (Fig. 5) but also having clearly identified the phases associated with this phase diagram, it is appropriate to investigate the possible physical origin, or mechanism, for this apparent similarity

between pressure applied to a Sn-grown crystal of $CaFe_2As_2$ and annealing of FeAs-grown crystals.

A starting point for this search for a mechanism can be found in a subset of the observations made above. The as-grown crystals from FeAs solution are far more brittle than either the Sn-grown crystals or the FeAs-grown crystals after a 400°C anneal. This qualitative observation hints at some higher concentration of defects in the as-grown crystals that lead to embrittlement. In addition, both the Mössbauer and NMR measurements find broader line shapes associated with the spectra from the as-grown samples, indicating that there may be a greater degree of disorder in them than in the crystal annealed at 400(500)°C.

In order to examine the distribution of defects at a nanoscale level, TEM measurements were carried out on both as-grown (quenched from 960°C) samples as well as samples that had been annealed at 500°C for a week. The as-grown sample [Fig. 12(a)] shows a pervasive tweedlike pattern with ~40 nm separation of features. The selected area diffraction pattern, [inset, Fig. 12(a)] shows only the [0,0,1] zone axis pattern consistent with the $CaFe_2As_2$ compound and no additional reflections or streaking indicative of a superlattice or a highly defective (intercalated) lattice. These very long but thin features are orthogonal and are approximately parallel to the $\{h,0,0\}$ planes as best can be determined in this orientation of the sample. The thinnest regions of the sample did not exhibit these features, consistent with the ease at which these samples were damaged by ion milling. (Milling above 3 keV and not cooling with liquid nitrogen resulted in significant milling artifacts.) The thickness of the foils where these features are present, and the lattice strain they cause, prevent atomic resolution imaging at this point. However, tilting experiments and imaging with the principle reflections did reveal the two-dimensional nature of these thin lamellae. These features were consistent throughout all the thin area of the sample, although in some regions one variant may dominate over the other and in some regions interpenetrating lamellae were observed, as shown in Fig. 12(a). Occasional dislocations were observed, but they did not dominate the microstructure.

The sample annealed at 500°C for 1 week appears completely different. Here we observed a very smooth contrast across the thin region when tilting and uniformly distributed small lenticular precipitates about 25 to 100 nm in width and with a length to width aspect about 5:1 [Fig. 12(b)]. These precipitates are also fairly uniformly separated, ~500 to 1000 nm, and have their long axis parallel to the $\{h,0,0\}$, as was observed in the tweed pattern of the 960°C quenched sample. Dislocations in the matrix are commonly observed to emanate from the interface between the precipitates and the matrix typically near the ends of the precipitate where stresses would be higher if there are differences in coefficients of thermal expansion. The SADP is nearly identical to the as-grown sample but here the precipitates are large enough for diffraction analysis. The convergent beam electron diffraction (CBED) pattern [right inset in Fig. 12(b)] produces disks rather than spots due to how the pattern is formed, but it is clear that the pattern is identical to that of the matrix. The fact that the SADP did not show any splitting of spots when including the precipitates and the matrix in the same sample

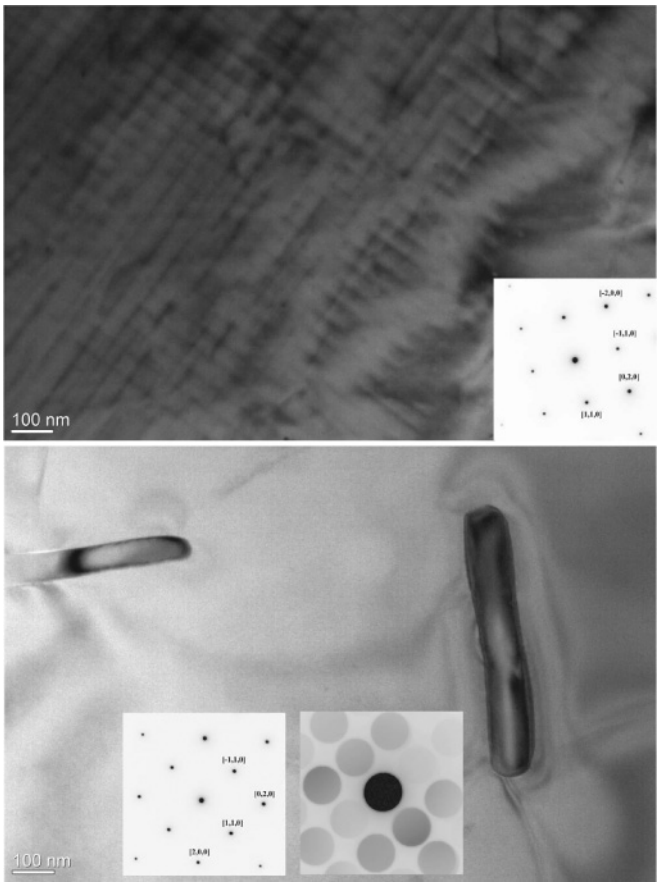

FIG. 12. (a) TEM micrograph of the as-grown and quenched sample. The fine tweedlike pattern is due to thin platelets of a second phase which are coherent with the matrix and parallel the $\{h,0,0\}$ planes. The inset on the right is the SADP from this image area showing expected lattice reflections for a [0,0,1] zone axis for the 122 compound. Note the absence of streaking or extra reflections as discussed in the text. (b) TEM micrograph of the sample annealed at 500°C for 1 week at the same magnification and zone axis orientation as the as-grown sample above. Note that the rectangular precipitates are oriented along the same $\{h,0,0\}$ planes as the finer features above. The inset on the left shows the SADP of the matrix and precipitates while the right inset is a CBED of only the precipitate phase showing nearly the same orientation and d spacing as the matrix 122 phase.

area would suggest that in this orientation the two lattices are nearly coherent. EDS also indicated that the precipitate phase does not contain Ca. Efforts to identify the precise chemistry and structure of this second phase are ongoing but it should be noted that the basal plane dimensions of the $CaFe_2As_2$ and the tetragonal $AsFe_2$ (space group $P4/nmm$, #129) are within 5% and have very similar [0,0,1] diffraction patterns. A gross estimate of the impurity phase area in less than 5% of the total sample, giving a gross idea of how much extra Fe and As is trapped in the sample when it is initially quenched from 960°C.

The similarity in the orientation and lack of distinguishing features in the diffraction between the as grown samples and the samples that were annealed suggests that there is a similarity in chemistry and structure between the tweed strain fields

and coarser precipitates in these two samples and the difference is simply one of length scale. An epitaxial relationship would lower the energy barrier for nucleation and allow a second phase to form more readily if thermodynamically stable. Annealing at moderate temperatures but within a two-phase field would promote growth of the second phase to reduce the excess energy due to interfaces (i.e., Oswald ripening). The observations here are consistent with an increase in the width of formation of $CaFe_2As_2$ with respect to excess As and Fe at elevated temperatures which decreases monotonically with temperatures below 960°C.

Such a temperature-dependent solid solubility of excess Fe and As leads to the following (plausible) scenario. When the FeAs flux grown crystal is first quenched, there is little time for the excess As and Fe to come out of solution. In these single crystals, the grain dimensions (often millimeters to centimeters) are simply too large for diffusion to allow for the expulsion of these species to the grain boundaries. Energetically, it appears easiest to exsolve excess As and Fe epitaxially along the $\{h,0,0\}$ planes. Differences in their unit cell size as well as their coefficients of thermal expansion (CTE) can lead to significant stresses at the interfaces between the $CaFe_2As_2$ majority phase and the finely dispersed Fe/As-based second phase. If, as Fig. 12(a) would suggest, domains of $CaFe_2As_2$, about 40 nm on a side, are surrounded by nearly coherent second phase resulting in a significant volume fraction of interfaces or regions strained by interfaces, then the magnitude of the stress would be dependent on the volume fraction of the $CaFe_2As_2$ in these strained regions.

If there is a temperature dependence of the solubility of the excess As and Fe, then quenching from lower temperatures would result in a smaller fraction of finely dispersed second phase, the remaining excess As and Fe being sequestered in larger precipitates whose insignificant surface to volume ratio would have little impact on the matrix [as is the case in Fig. 12(b)]. This smaller amount of finely dispersed precipitate would lead to a smaller average strain (or pressure) on the sample, leading to an effective correlation between P and T_a. Since the initial quench of the large crystals from the flux essentially locks in the excess As and Fe, the subsequent processing history determines the size and distribution of the second phase and thereby determines the amount of strain in the sample.

Alternatively, if there is a temperature dependence of the solubility of excess As and Fe then quenching from lower temperatures could result in a systematic control of how much As and Fe are trapped (metastably) in a $CaFe_{2+\delta}As_{2+\gamma}$ phase. Within this hypothesis the excess As and Fe remaining in the $CaFe_2As_2$ phase would be the parameters controlling the value of T^* and nature of the low-temperature ground state. Whereas this hypothesis cannot be ruled out within the current data set, the clear, tweedlike patterns seen in Fig. 12(a) are more consistent with the strain field from a nanoprecipitate.

Further exploration of this hypothesis requires confirmation of the second-phase crystal structure and its chemistry and determination of the CTE and bulk moduli of these two phases. In addition, returning to the initial motivations for this study: given that annealing of as grown samples seems to lead to small changes in the transition temperatures of $BaFe_2As_2$-based compounds[17,18] and given that $CaFe_2As_2$ is much more pressure or strain sensitive than $BaFe_2As_2$, it is worth exploring the implications of our current findings. If we speculate that a similar width of formation exists in $BaFe_2As_2$ (or for that matter $SrFe_2As_2$) and that low-temperature annealing can lead to similar effects as those we present here, then, based on the existing P-T phase diagrams,[27] an effective pressure of ~0.4 GPa on $BaFe_2As_2$ or $SrFe_2As_2$ would lead only to shifts in T^* of a few K, consistent with what has been observed.[17,18] Based on this analysis, TEM measurements on as-grown and annealed crystals of $BaFe_2As_2$, as well as $SrFe_2As_2$, to check for similar, annealing temperature-dependent microstructure are in order.

IV. CONCLUSIONS

We have found a remarkably large response of the transition temperature of $CaFe_2As_2$ single crystals grown from excess FeAs to annealing or quenching temperature. Whereas crystals that are annealed at 400°(500°)C exhibit a first-order phase transition from a high-temperature tetragonal to a low-temperature orthorhombic-antiferromagnetic state near 170 K (similar to what has been found in the original Sn-grown single crystals[1,2]), crystals that have been quenched from 960°C exhibit a transition from a high-temperature tetragonal phase to a low-temperature, nonmagnetic, collapsed tetragonal phase below 100 K. We have been able to demonstrate that the transition temperature can be reduced in a monotonic fashion by varying the annealing or quenching temperature from 400° to 850°C with the low-temperature state remaining antiferromagnetic for transition temperatures larger than 100 K and becoming collapsed tetragonal, nonmagnetic for transition temperatures below 90 K. This suppression of the orthorhombic, antiferromagnetic phase transition and its ultimate replacement with the collapsed tetragonal, nonmagnetic phase is similar to what has been observed for Sn-grown single crystals of $CaFe_2As_2$ under hydrostatic pressure.[9] This similarity is summarized in Fig. 5(b).

TEM studies of the as-grown (quenched from 960°C) and annealed crystals indicate that there is a temperature-dependent width of formation of $CaFe_2As_2$ with a decreasing amount of excess Fe and As being soluble in the single crystal at lower annealing temperatures. On one extreme, samples quenched from 960°C have finely divided strain structure with characteristic length scales and spacings of less than 50 nm. On the other extreme, samples annealed at 500°C have clearly identifiable Ca-free crystalline inclusions with dimensions of $\sim 70 \times 500$ nm^2 that are separated by 500 to 1000 nm. These images make it clear that when the sample is quenched from 960°C it is possible to think of some average, near uniform strain throughout the sample associated with the overlapping strain fields of this fine precipitate. It is this strain that appears to be giving rise to the dramatic suppression of T^*, in, apparently, a manner similar to that hydrostatic pressures of ~0.4 GPa.

Finally, it is worth noting that, as was the case with hydrostatic pressure applied by helium pressure medium,[9] there is no indication of superconductivity, even in trace amounts. This would be consistent with the idea that superconductivity comes

from the poorly defined strains associated with the onset of the collapsed phase in a confined (solidified pressure medium) volume. Given that these measurements are at ambient pressure, this is not the case. By the same token, though, given that we can essentially mimic the key effects of hydrostatic pressure via variation of T_a, the collapsed tetragonal phase, as well as the orthorhombic, antiferromagnetic phase with intermediate T^* values, is open to measurements at ambient pressure. This should make detailed thermodynamic, microscopic, and spectroscopic measurements across the phase space outlined in Fig. 5(b) much more accessible.

ACKNOWLEDGMENTS

We thank D. Robinson for his excellent technical support of the x-ray diffraction study. This work was supported by the US Department of Energy, Office of Basic Energy Science, Division of Materials Sciences and Engineering. Ames Laboratory is operated for the US Department of Energy by Iowa State University Under Contract No. DE-AC02-07CH11358. Work at McGill University was supported by grants from the Natural Sciences and Engineering Research Council of Canada and Fonds Québécois de la Recherche sur la Nature et les Technologies.

[1] N. Ni, S. Nandi, A. Kreyssig, A. I. Goldman, E. D. Mun, S. L. Bud'ko, and P. C. Canfield, Phys. Rev. B**78**, 014523 (2008).

[2] P. C. Canfield, S. L. Bud'ko, N. Ni, A. Kreyssig, A. I. Goldman, R. J. McQueeney, M. S. Torikachvili, D. N. Argyriou, G. Luke, and W. Yu, Physica C **469**, 404 (2009).

[3] A. I. Goldman, D. N. Argyriou, B. Ouladdiaf, T. Chatterji, A. Kreyssig, S. Nandi, N. Ni, S. L. Bud'ko, P. C. Canfield, and R. J. McQueeney, Phys. Rev. B **78**, 100506 (2008).

[4] G. Wu, H. Chen, T. Wu, Y. L. Xie, Y. J. Yan, R. H. Liu, X. F. Wang, J. J. Ying, and X. H. Chen, J. Phys. Condens. Matter **20**, 422201 (2008).

[5] F. Ronning, T. Klimczuk, E. D. Bauer, H. Volz, and J. D. Thompson, J. Phys. Condens. Matter **20**, 322201 (2008).

[6] Milton S. Torikachvili, Sergey L. Bud'ko, Ni Ni, and Paul C. Canfield, Phys. Rev. Lett. **101**, 057006 (2008).

[7] A. Kreyssig, M. A. Green, Y. Lee, G. D. Samolyuk, P. Zajdel, J. W. Lynn, S. L. Bud'ko, M. S. Torikachvili, N. Ni, S. Nandi, J. B. Leão, S. J. Poulton, D. N. Argyriou, B. N. Harmon, R. J. McQueeney, P. C. Canfield, and A. I. Goldman, Phys. Rev. B **78**, 184517 (2008).

[8] A. I. Goldman, A. Kreyssig, K. Prokes, D. K. Pratt, D. N. Argyriou, J. W. Lynn, S. Nandi, S. A. J. Kimber, Y. Chen, Y. B. Lee, G. Samolyuk, J. B. Leão, S. J. Poulton, S. L. Bud'ko, N. Ni, P. C. Canfield, B. N. Harmon, and R. J. McQueeney, Phys. Rev. B **79**, 024513 (2009).

[9] W. Yu, A. A. Aczel, T. J. Williams, S. L. Bud'ko, N. Ni, P. C. Canfield, and G. M. Luke, Phys. Rev. B **79**, 020511 (2009).

[10] Hanoh Lee, Eunsung Park, Tuson Park, V. A. Sidorov, F. Ronning, and E. D. Bauer, and J. D. Thompson, Phys. Rev. B **80**, 024519 (2009).

[11] M. S. Torikachvili, S. L. Bud'ko, N. Ni, P. C. Canfield, and S. T. Hannahs, Phys. Rev. B **80**, 014521 (2009).

[12] K. Prokes, A. Kreyssig, B. Ouladdiaf, D. K. Pratt, N. Ni, S. L. Bud'ko, P. C. Canfield, R. J. McQueeney, D. N. Argyriou, and A. I. Goldman, Phys. Rev. B **81**, 180506 (2010).

[13] Tuson Park, Eunsung Park, Hanoh Lee, T. Klimczuk, E. D. Bauer, F. Ronning, and J. D. Thompson, J. Phys. Condens. Matter **20**, 322204 (2008).

[14] S. L. Bud'ko, P. C. Canfield, C. H. Mielke, and A. H. Lacerda, Phys. Rev. B **57**, 13624 (1998).

[15] C. Petrovic, S. L. Bud'ko, and P. C. Canfield, J. Magn. Magn. Mater. **247**, 270 (2002).

[16] D. K. Pratt, Y. Zhao, S. A. J. Kimber, A. Hiess, D. N. Argyriou, C. Broholm, A. Kreyssig, S. Nandi, S. L. Bud'ko, N. Ni, P. C. Canfield, R. J. McQueeney, and A. I. Goldman, Phys. Rev. B **79**, 060510 (2009).

[17] C. R. Rotundu, B. Freelon, T. R. Forrest, S. D. Wilson, P. N. Valdivia, G. Pinuellas, A. Kim, J.-W. Kim, Z. Islam, E. Bourret-Courchesne, N. E. Phillips, and R. J. Birgeneau, Phys. Rev. B **82**, 144525 (2010).

[18] K. Gofryk, A. S. Sefat, M. A. McGuire, B. C. Sales, D. Mandrus, T. Imai, J. D. Thompson, E. D. Bauer, and F. Ronning, arXiv:1009.0954v1 (2010), unpublished.

[19] N. Ni, M. E. Tillman, J.-Q. Yan, A. Kracher, S. T. Hannahs, S. L. Bud'ko, and P. C. Canfield, Phys. Rev. B **78**, 214515 (2008).

[20] P. C. Canfield and Z. Fisk, Philos. Mag. B **65**, 1117 (1992).

[21] A. Kreyssig, S. Chang, Y. Janssen, J. W. Kim, S. Nandi, J. Q. Yan, L. Tan, R. J. McQueeney, P. C. Canfield, and A. I. Goldman, Phys. Rev. B **76**, 054421 (2007).

[22] N. N. Greenwood and T. C. Gibb, *Mössbauer Spectroscopy* (Chapman & Hall, London, 1971), p. 67.

[23] X. Y. Miao, S. L. Bud'ko, and P. C. Canfield, J. Alloys Compd. **338**, 13 (2002).

[24] G. C. Carter, L. H. Bennet, and D. K. Kahan (eds.), *Metallic Shift in NMR* (Pergamon, New York, 1977).

[25] S.-H. Beak, N. J. Curro, T. Klimczuk, E. D. Bauer, F. Ronning, and J. D. Thompson, Phys. Rev. B **79**, 052504 (2009).

[26] S. Kawasaki, T. Oka, T. Tabuchi, X. F. Wang, X. H. Chen, G-Q. Zhen, J. Phys. Chem. Solid (in press).

[27] E. Colombier, S. L. Bud'ko, N. Ni, and P. C. Canfield, Phys. Rev. B **79**, 224518 (2009).